Journal of Materials Chemistry A

Accepted Manuscript

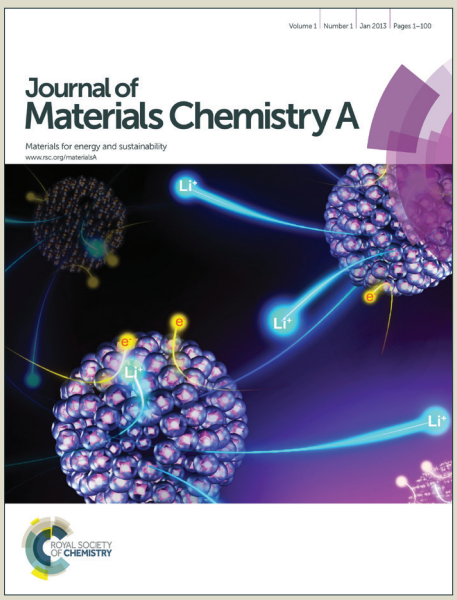

ROYAL SOCIETY OF CHEMISTRY

www.rsc.org/materialsA

A new aspect of Chevrel compounds as a positive electrode for magnesium battery

T. Ichitsubo,[1]* S. Yagi,[2] R. Nakamura,[1] Y. Ichikawa,[2] S. Okamoto,[1] K. Sugimura,[1] T. Kawaguchi,[1] A. Kitada,[1] M. Oishi,[3] T. Doi,[4] E. Matsubara[1]

[1] *Department of Materials Science and Engineering, Kyoto University, Kyoto 606-8501, Japan*
[2] *Nanoscience and Nanotechnology Research Center, Osaka Prefecture University, Osaka 599-8570, Japan*
[3] *Graduate School of Engineering, Kyoto University, Kyoto 606-8501, Japan*
[4] *Department of Molecular Chemistry and Biochemistry, Doshisha University, Kyoto 610-0321, Japan*

(Dated: June 30, 2014)

Chevrel compounds are regarded as positive-electrode materials of a magnesium rechargeable battery, but their redox potential is about 1.2 V vs. Mg/Mg^{2+}. In this work, we show logically and experimentally a new aspect of the Chevrel compounds that their redox potential can be as high as about 2-3 V vs. Mg/Mg^{2+}. A crucial basis on this aspect is that Cu cations can be extracted from $Cu_xMo_6S_8$ around 1.2-1.6 V vs. Mg/Mg^{2+} in the conventional electrolyte (Grignard-reagent/tetrahydrofuran) while the anodic dissolution of Cu metal can occur above about 1.7 V vs. Mg/Mg^{2+} in the same electrolyte, which means that the chemical potential of Cu in the Chevrel compounds is higher than that in pure Cu metal. This thermodynamic conflict inevitably compels us to consider a certain interaction with the solvent other than the simple deintercalation from the compound, which is discussed through the paper. With the use of large molecule solvent or ionic liquids, we have observed an intriguing relaxation phenomena, where the cations move to find more stable sites, which directly indicates that the Chevrel compounds have several sites for cations.

1. INTRODUCTION

The energy density of lithium ion batteries (LIBs) has been enlarged year by year, but recently its growing rate tends to be saturated. Since lithium metal has a high gravimetric/volumetric capacity and the lowest electrode potential (−3.05 V vs. SHE),[1, 2] if lithium metal is available as a negative electrode instead of carbonaceous materials currently used, the lithium battery would have shown a significantly high energy density. However, actually lithium metal cannot be adopted for LIBs due to the well-known fatal problem on the dendritic growth of lithium during charge, which leads to a dangerous short circuit.[3] In order to overcome this problem, in late years, non-noble polyvalent metals (such as Ca, Mg, Al) are tried to be used as a negative electrode for polyvalent-metal rechargeable batteries.[4] This is because polyvalent metals can be expected to work as a potential negative electrode, whose capacity is much higher (e.g., 2234 mAh g^{-1} for Mg) than that of carbonaceous material (about 370 mAh g^{-1}) used in the current LIBs. As demonstrated by the previous works,[5–11] the magnesium deposition can be done with the Grignard regent (R-MgX, R: Alkyl or aryl group, X: halogen) and AlR_xCl_{3-x} salt in the tetrahydrofuran (THF) solvent, and the coulombic efficiency associated with cathodic electrodeposition and anodic dissolution of magnesium in the Grignard-reagent/THF electrolyte is high. More importantly, unlike Li metal, magnesium can be electrodeposited rather smoothly without the dendritic growth that causes a fatal concern about a short circuit in the battery.[12–15]

However, comparing to the research field in LIBs, where we can opt many combinations of positive/negative electrodes and electrolytes, the magnesium rechargeable battery (MRB) study is quite limited due to few choices in combination of the positive electrode materials and electrolytes. Because, despite that several candidates for the positive electrode materials of MRBs have been reported,[16–18] currently only Chevrel compounds substantiated by Aurbach et al.[5–10] are known to show superior intercalation/deintercalation characteristics with an excellent cyclability. This is generally attributed to the sluggish topotactic motion of the polyvalent cations in the crystal structure due to strong coulomb restraint. In the Chevrel structure the diffusion of Mg cations can occur but, unfortunately, even when the Chevrel compounds are used as the positive electrode, it can deliver less voltage (about 1.2 V) in comparison with the cell voltage of LIBs (about 4 V).[19]

In this work, we elicit a new aspect of the Chevrel compounds that the redox potential of the Mo_6S_8 cluster in the compounds can possess a high redox potential of about 2-3 V vs. Mg/Mg^{2+}. For a realistic solution toward the practical application of MRBs, we try to reveal why the Chevrel compounds show such a low redox potential as about 1.2 V vs. Mg/Mg^{2+} in the conventional battery system and demonstrate how to exploit their high redox potential, with our appreciation to the notable trailblazing work by Aurbach et al.[5]

*Email: tichi@mtl.kyoto-u.ac.jp

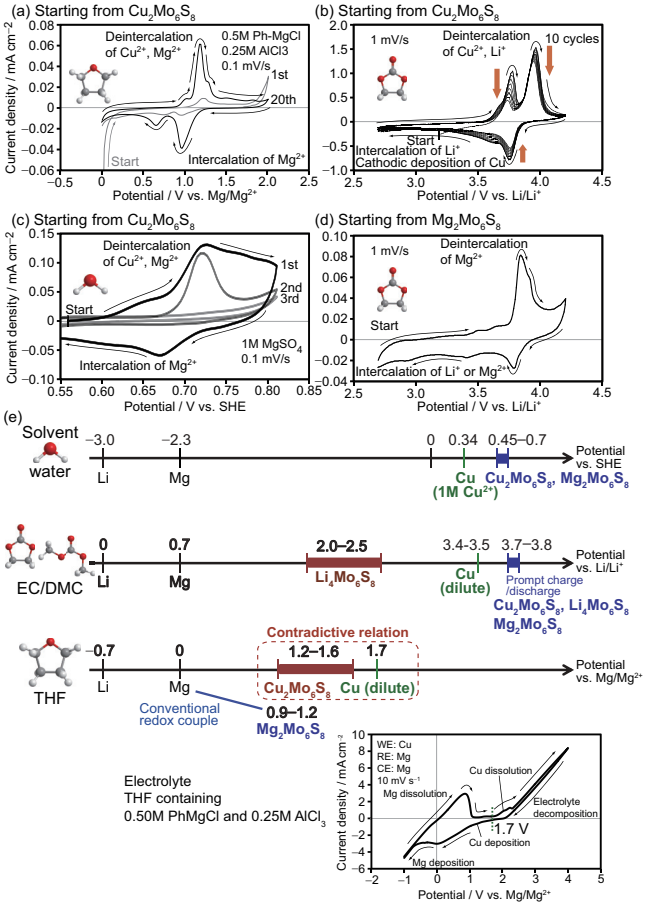

FIG. 1: Cyclic voltammograms for various electrolytes of the Chevrel compounds, (a) $Cu_2Mo_6S_8$ in phenylmagnesium chloride/THF electrolyte with $AlCl_3$, (b) $Cu_2Mo_6S_8$ in $LiPF_6$/EC-DMC electrolyte, (c) $Cu_2Mo_6S_8$ in 1M $MgSO_4$ aqueous solution, (d) $Mg_2Mo_6S_8$ in $LiPF_6$/EC-DMC electrolyte, and (e) the summary of the redox potentials of Chevrel phase observed in various electrolytes. The cyclic voltammogram of Cu metal in phenylmagnesium chloride/THF electrolyte with $AlCl_3$[14] is also shown for reference. EC and DMC denote ethylene carbonate and dimethyl carbonate, respectively. In (b), the redox-peak current decreases with the increase in cycle number as indicated by arrows.

2. SEVERAL MYSTERIES OBSERVED IN CHEVREL PHASE

Figure 1(a)-(d) show typical cyclic voltammograms obtained for Chevrel compounds ($Cu_2Mo_6S_8$, $Mg_2Mo_6S_8$, etc) in various electrolytes (THF, EC-DMC, aqueous solvent), and these electrochemical behaviors of the Chevrel compounds are summarized in Fig. 1(e). Especially, it is striking that the anodic dissolution (or electrodeposition) of Cu metal occurs above $E_{Cu^{2+}/Cu} \approx 1.7$ V vs. Mg/Mg^{2+} in Grignard-reagent/THF electrolyte,[13, 14] while Cu cations can be extracted from the Chevrel crystal at a lower value such as about 1.2 V in the same electrolyte, as shown in Fig. 1(a). In a more limited CV scan between 0 V and 1.6 V ($< E_{Cu^{2+}/Cu}$), the above fact was also confirmed; see in Supplementary Fig. S1. As far as we consider only the rocking-chair mechanism (i.e., the electrochemical reaction does not depend on the concentration of electrolyte, etc), the above fact means that the chemical potential of the Cu element in the Chevrel phase, μ^{CP}_{Cu}, is higher than that of pure Cu metal, μ^{0}_{Cu}, i.e.,

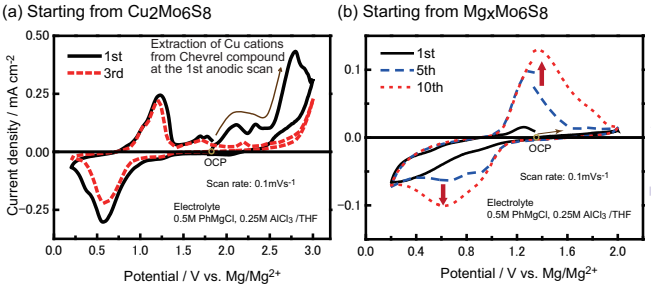

FIG. 2: Cyclic voltammograms for various electrolytes of the Chevrel compounds, (a) $Cu_2Mo_6S_8$ and (b) $Mg_xMo_6S_8$ in phenylmagnesium chloride/THF electrolyte with $AlCl_3$. Only in the first anodic scan from the OCP value of about 1.7 V vs. Mg/Mg^{2+} in (a), the anodic peaks attributed to the deintercalation of Cu cations can be observed around 2-3 V vs. Mg/Mg^{2+}, after that such a anodic peak was absent. Also in $Mg_xMo_6S_8$, the first anodic scan cannot extract the Mg cations from the crystal, and after sevral scans gradually the cations can be extracted from the crystal.

$$\mu^{0}_{Cu} < \mu^{CP}_{Cu} \quad \text{(in THF)}, \tag{1}$$

which is crucially contradictive to thermodynamics and deeply discussed in Appendix. In general, the chemical potentials of the constitutive elements in a compound should be naturally lower than those in pure elements. According to literature,[20] the intercalation/deintercalation potential of Cu cations in $Cu_xMo_6S_8$ is about 0.45-0.7 V vs. SHE in 1M $CuSO_4$ aqueous solution under an ambient condition, and is higher than the redox potential of Cu metal (about 0.34 V vs. SHE), which indicates that $Cu_2Mo_6S_8$ is thermodynamically stable at room temperature. Therefore, this thermodynamic contradictive relation, eq. (1), inevitably compels us to examine *a certain interaction with the solvent* other than the simple deintercalation from the compound. (Incidentally, how to understand the chemical potential of zero-valence element in an ionic crystal was described in detail in our previous paper.[21])

Although the above-mentioned phenomena sufficiently deserves to be reexamined in terms of the electrochemical reaction of the Chevrel compounds, it is worthwhile to mention other several features here. As before, Cu cations can be extracted from $Cu_2Mo_6S_8$ at a redox po-

tential as low as about 1.2-1.6 V vs. Mg/Mg^{2+}. However, as seen in Fig. 1(b) and (c), the deintercalation of Cu ions from $Cu_2Mo_6S_8$ and intercalation of cations (Li, Mg or Cu ions) occur at about 3.7 V vs. Li/Li^+ (∼3.0 V vs. Mg/Mg^{2+}) in the conventional $LiPF_6$/EC-DMC electrolyte, and at about 0.7 V vs. SHE (∼3.0 V vs. Mg/Mg^{2+}) in an aqueous solution. Similarly, in Fig. 1(d), the deintercalation of Mg ions from $Mg_2Mo_6S_8$ and intercalation of Li ions or Mg ions occur at about 3.7 V vs. Li/Li^+ (∼3.0 V vs. Mg/Mg^{2+}). (Note here that the potential values in the parentheses are for reference.) These redox potentials are not contradictive to thermodynamics, and very consistent with the previously reported potential values.[20] In addition, a first principle calculation[22] reported that the cell voltage is about 2 V.

Here, in order to check the influences by the different scales due to the various electrolytes, we have conducted the CV measurements for $Cu_2Mo_6S_8$ in phenylmagnesium chloride/THF electrolyte with $AlCl_3$ by a prompt anodic scan from the open circuit potential (OCP), and measured the cycle dependence of CV for a pristine $Mg_xMo_6S_8$ sample; see Fig. 2(a) and (b). As is expected from the above argument, Cu cations can be extracted from the Chevrel crystal above 2 V vs. Mg/Mg^{2+} in the first anodic scan (but accompanied by anodic decomposition of the electrolyte), being much higher than the conventional value about 1-1.2 V vs. Mg/Mg^{2+}. Incidentally, if the rocking-chair mechanism holds, as understood from eqs. (17)-(19) in Appendix, the deintercalation potential of Cu from $Cu_xMo_6S_8$ in phenylmagnesium chloride/THF electrolyte with $AlCl_3$ must be about 1.8-2.1 V vs. Mg/Mg^{2+} so as to be consistent with the results by Schöllhorn et al.;[20] these values are found to be comparable to the result in Fig. 2(a). Thus, we can discuss the potential values, even if we use different electrolytes.[23] In addition, as seen in Fig. 2(b), it is noteworthy that Mg cations can be gradually extracted from the crystal after several cycles, which means that it takes certain duration till the extraction of cations can be done sufficiently. This is discussed in the later section.

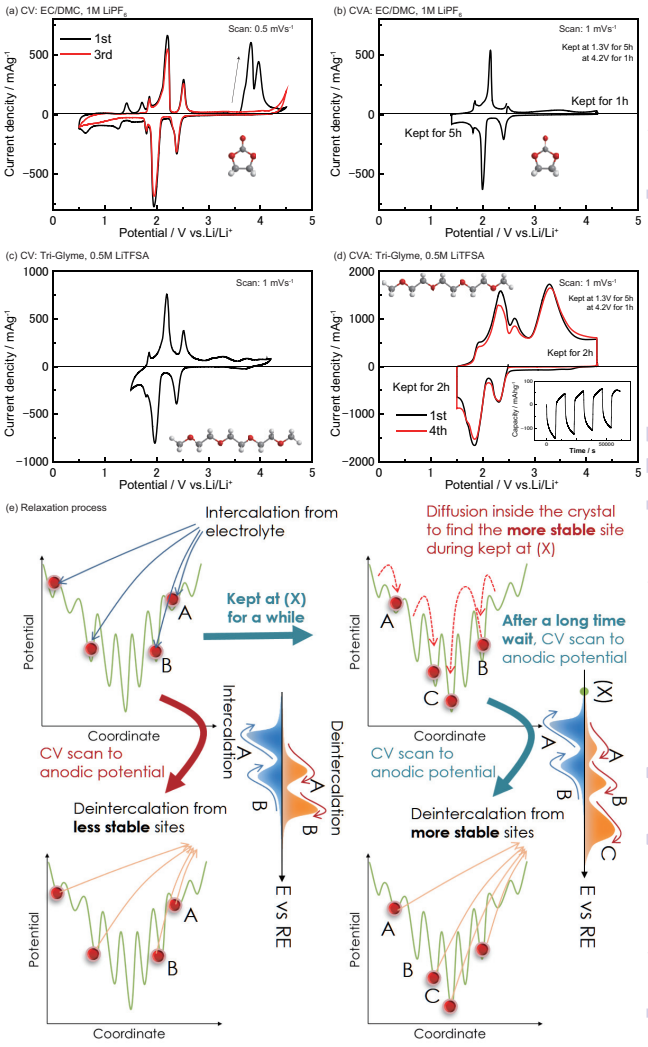

FIG. 3: Current versus potential profiles obtained by cyclic voltammetry (CV) and cyclic voltammetry with chronoamperometry (CVA), (a) CV for $Cu_2Mo_6S_8$ (0.5 mV/s), (b) CVA for Mo_6S_8 in $LiPF_6$/EC-DMC electrolyte (1 mV/s), (c) CV for Mo_6S_8 (1 mV/s), (d) CVA for Mo_6S_8 in LiTFSA/triglyme electrolyte (1 mV/s), and (e) schematic illustration explaining the relaxation process by diffusion in the crystal to find the more stable sites for cations in (d). The active material of Mo_6S_8 was prepared by leaching using condensed hydrochloric acid (c-HCl).

3. RELAXATION PHENOMENA OBSERVED IN CHEVREL PHASE

As discussed later in details, as a certain interaction with the electrolyte solvent, *which must be considered, in this case, to circumvent the thermodynamic contradiction*, here we suppose that solvent molecules may infiltrate into the Chevrel crystal to hinder the proper intercalation/deintercalation of the cations. If the solvent does not infiltrate into the crystal, the deep potential sites would be exploited for a high voltage battery. With this in mind, we have conducted several electrochemical tests for the Chevrel compounds on the assumption that solvents of "larger molecules" or "ionic liquid" cannot infiltrate into the crystal.

3.1. Li intercalation/deintercalation

We first tried to use an electrolyte consisting of triethylene glycol dimethyl ether (triglyme) solvent with a LiTFSA salt [TFSA: bis(trifluoromethanesulfonyl)amide, $N(CF_3SO_2)_2^-$]; the characteristics of the electrolyte is shown in Supplementary Fig. S2.

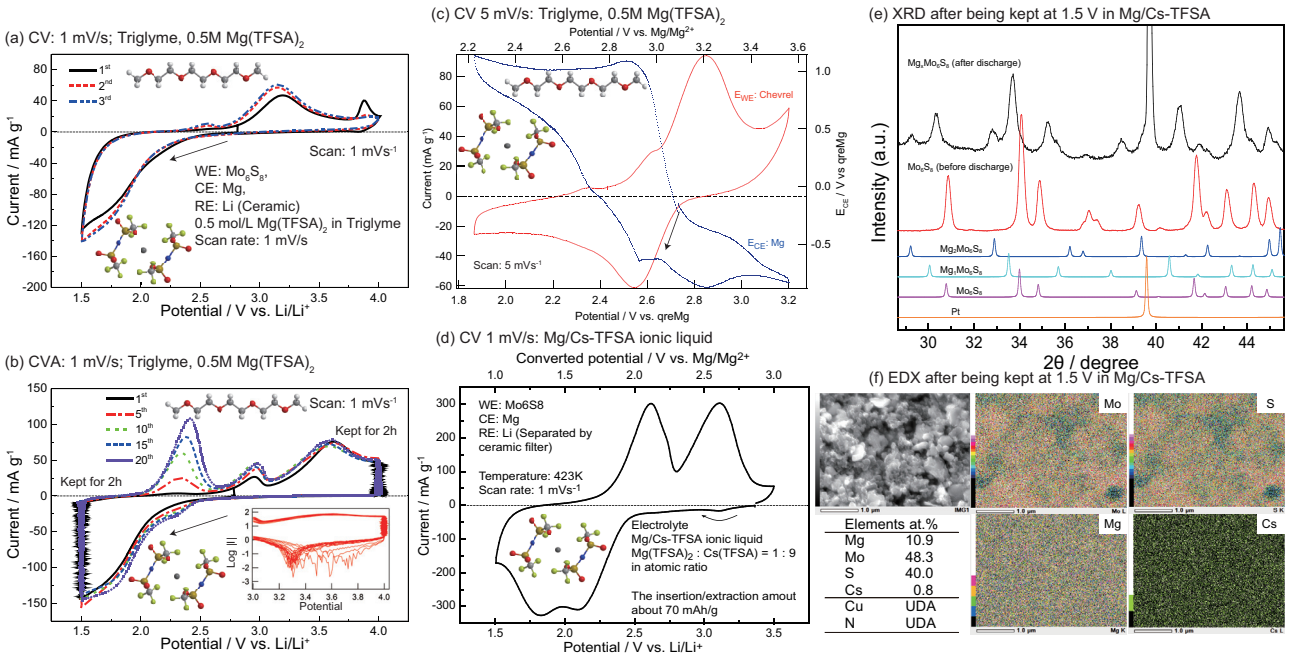

FIG. 4: Current versus potential profiles obtained by CV and CVA electrochemical tests; (a) CV for Mo_6S_8 in $Mg(TFSA)_2$/triglyme electrolyte (1 mV/s), (b) CVA for Mo_6S_8 in $Mg(TFSA)_2$/triglyme electrolyte (1 mV/s) and Tafel plot of the CVA profile (inset) (c) CV at a relatively fast scan rate (5 mV/s) for Mo_6S_8 in $Mg(TFSA)_2$/triglyme electrolyte, (d) CV (1 mV/s) for Mo_6S_8 in $Mg(TFSA)_2$/CsTFSA electrolyte, where the atomic ratio of cations are $Mg : Cs = 1 : 9$, (e) XRD profiles obtained before/after discharge at 1.5 V vs. Li/Li^+ for 24h in $Mg(TFSA)_2$/CsTFSA electrolyte, and (f) EDX element mapping and composition after the discharge, where "UDA" means the elements that were undetected automatically by our SEM-EDX instrument. In (a) and (b), Li metal was used for the reference (Li in 0.5M LiTFSA), where Li reference was separated by the porous ceramic glass, and in (c) Mg metal was used for the quasi reference (i.e., the Mg reference in the same electrolyte), and in (d) Li metal in a separated tube with ceramic filter was used for the reference (0.5 M LiTFSA/DEME-TFSA). The CVA test in (b) was done after the CV test in (a) with the use of the same beaker cell.

Figure 3 shows the current-potential profiles (voltammograms) obtained by the cyclic voltammetry (CV) and cyclic voltammetry with chronoamperometry (CVA) at the potential edges in the sweep. In using $LiPF_6$/EC-DMC electrolyte, as before, Cu cations are extracted at 3.7 V vs. Li/Li^+ in the first scan from the OCP point to the anodic side in Fig. 3(a). After the deintercalation of Cu cations, the EC molecule may infiltrate into the crystal, and as a consequence the cations can be inserted/extracted at lower potential values (or co-intercalation of solvent may occur at a lower potential). Even for the CVA mode (kept at 1.5 V vs. Li/Li^+ for 5h in the chronoamperometry mode), the CVA profile in Fig. 3(b) is substantially similar to the CV profile in Fig. 3(a). However, in contrast, in using the triglyme solvent, the CV profile in Fig. 3(c) is very similar to those obtained for EC-DMC solvent, but CVA profile (kept at 1.5 V vs. Li/Li^+ for 2h) in Fig. 3(d) is very different from the other profiles; a new anodic peak appears at a higher potential. As illustrated in Fig. 3(e), the cations can move to find the more stable sites, that is, a certain relaxation occurs, while kept at 1.5 V vs. Li/Li^+ for 2h (in the chronoamperometry mode), since the large solvent molecule such as triglyme does not infiltrate to occupy the most stable sites in the crystal. On the contrary, in the case of small molecule solvent such as EC-DMC, if the solvent molecules infiltrate to occupy the stable site in the crystal, the cations cannot move to find the more stable site even when the sample is kept at 1.5 V vs. Li/Li^+ for about 5h. Thus, it is experimentally concluded that the Chevrel structure has many local potential minima in the crystal for the cations. If the infiltration of solvent does not occur, the redox potential of the Chevrel phase would be as high as 2-3 V vs. Mg/Mg^{2+}.

In the thermal equilibrium, the site occupancy p_i of the cations at the potential energy E_i (corresponding to the charge/discharge amount at each potential) in the crystal would be given by

$$p_i = \frac{w_i \exp(-E_i/kT)}{\sum_i w_i \exp(-E_i/kT)},$$

where $\sum_i w_i \exp(-E_i/kT)$ means the small partition function, the summation is done within the crystal, w_i is the number of sites at the energy E_i, k is the Boltzmann constant, and T is the temperature. The number of the sites w_i is an important value of the crystal structure,

and generally it would be large at shallow potential sites, while w_i would be minimum at the deepest potential site. Since the insertion process of cations occurring in the cathodic reaction is time-dependent, the cations can easily detect the moderate sites that has large w_i. Thus, in terms of kinetics, the cathodic reaction can be different from the anodic reaction in the CVA profile.

3.2. Mg intercalation/deintercalation

Figure 4 shows the results obtained with the use of electrolytes for the magnesium battery, where we used a large molecule solvent, $Mg(TFSA)_2$/triglyme electrolyte[24, 25] and ionic liquid $Mg(TFSA)_2$/CsTFSA electrolyte.[26, 27] The CV profile associated with the electrodeposition of magnesium is shown in Supplementary Fig. S3. Incidentally, we often use a Li-metal electrode in a separated glass tube with a ceramic filter as a reference electrode, and note that the Li cations are not included in the electrolyte.

As seen in Fig. 4(a), the cathodic reaction clearly occurs at a higher potential (about 2.7 V vs. Li/Li^+, i.e., about 2.0 V vs. Mg/Mg^{2+}) in $Mg(TFSA)_2$/triglyme electrolyte. Besides, in the CVA profile (kept at 1.5 V vs. Li/Li^+ for 2h) in Fig. 4(b), another higher potential peak newly appeared around 3-4 V vs. Li/Li^+ (peak top is about 3.7 V vs. Li/Li^+) as well as the case of Li in Fig. 3(d). Thus, the once-inserted Mg ions can move to the more stable potential sites in the Chevrel structure as well as Li ions. Furthermore, it is found that the cathodic reaction starts to occur at 3.3-3.7 V vs. Li/Li^+ by the Tafel plot of the CVA profile (inset in Fig. 4(b)). In order to make the cathodic reaction conspicuous, by using Mo_6S_8 powder prepared electrochemically, we have done the cyclic voltammetry at a faster rate of 5 mV/s in Fig. 4(c). By increase in the scan rate, the current density in the CV profile can be amplified (because it is about inversely proportional to the scan rate), and magnesium is concentrated by the diffusion control near/inside the particle surface at a small amount of its insertion, and consequently the peak is easily discernible in the cyclic voltammogram. Thus, the cathodic and anodic peaks at about 2.7 V vs. Mg quasi-reference are clearly observed, although the quasi reference is slightly passivated in $Mg(TFSA)_2$/triglyme electrolyte (about 0.4 V vs non-passivated Mg, for details, see Supplementary Fig. S3), which is close to the value by the previous first principle calculation.[22] The magnesium insertion at the higher potential (about 2.7-3 V vs. Mg/Mg^{2+}) seems to occur for the sample prepared without using water.

The operating temperature is a key control parameter of the cation distribution in terms of kinetics and thermodynamics. In the previous works by Hagiwara el al[26] and Oishi et al.[27], CsTFSA-based ionic liquid is stable at elevated temperature about 150-200 °C, and cathodic deposition and anodic dissolution of magnesium can be reversibly done in the electrolyte despite showing passivation.[27] Of course, since ionic liquids have no electroneutral solvent that can infiltrate into the crystal without any redox reactions, they are candidate for the use of Chevrel-phase positive electrode. The typical CV of the Chevrel phase at 180 °C is shown in Supplementary Fig. S4; also here the Cu cations are extracted at 3.7 V vs. Li/Li^+. Figure 4(d) shows a CV profile obtained at 150 °C (423 K) for Mo_6S_8 (WE) in using a $Mg(TFSA)_2$/CsTFSA electrolyte. After the CV test in Fig. 4(d), successively the sample was kept at 1.5 V vs. Li/Li^+ for 24h (discharge process). We have confirmed that Mg cations were mainly inserted into the crystal by XRD in Fig. 4(e) and EDX in Fig. 4(f), and Cs cations hardly insert into the Chevrel cyrstal, probably due to the large diameter of Cs cations. Although it is known that sole deposition of magnesium is difficult to occur in this electrolyte[28] (but the electrodeposition of Mg can be facilitated in $Mg(TFSA)_2$/CsTFSA-LiTFSA electrolyte[26, 27]), we have thus confirmed the electrolytic dissolution of Mg cations and TFSA anions in the $Mg(TFSA)_2$/CsTFSA electrolyte, and this is suitable for investigation of positive electrode materials of MRBs in that the mobility of Mg cations can be significantly enhanced at relatively high temperatures (around 150-200 °C).

4. DISCUSSION

From the present whole experimental results, the redox potential of Mo_6S_8 is surely close to 2-3 V vs. Mg/Mg^{2+} regardless of cation species. As was demonstrated in the previous work,[20] the intercalation/deintercalation potential must be higher than the redox potential of Cu metal (0.3 V vs. SHE) in terms of thermodynamics. Also in this case, the fact that Cu cations can be extracted at such a low potential (1.2 V vs. Mg/Mg^{2+}) in THF, which is lower than the anodic dissolution potential of Cu in THF (about 1.7 V vs. Mg/Mg^{2+}), is a conflict in terms of thermodynamics; see Appendix. *Now, what is happening on the Chevrel-compound electrode?*

Through this paper, we have assumed that solvent molecules infiltrate into the Chevrel crystal, as an interaction with the solvent that would affect the chemical potential of metal elements. Figures 3 and 4 strongly supports the present hypothesis, which indicates Chevrel compounds have deeper potential sites for cations. Even if they infiltrate at only surface, our discussion is not affected, and co-intercalation of solvent may also be a plausible candidate. When the solvent co-intercalation occurs into the rigid crystal, it is expected that the electrode potential should be lowered due to the strain energy effects.[29] Figure 5 shows the concept illustrating the potential versus coordinate in the crystal. The size of the

Mg-ring (or Cu-ring) in the crystal structure is very close to the size of polar THF or EC molecule, so that they may infiltrate into the crystal. When the solvent molecule occupies a region around the most stable site in the crystal as a disturbance of the cation site, the cations can be located only at the less stable sites. Consequently, the metal cations can be extracted from the crystal at a relatively low potential (i.e., from the less-stable site) by the potential sweep. Occasionally the solvent would incompletely infiltrate into the crystal, namely, only around the active-material surface; in such a case, the particle has a core not infiltrated by the solvent.

To detect some evidence of the solvent infiltration experimentally, we conducted the synchrotron (SPring-8) X-ray diffraction (XRD) measurements for $Cu_2Mo_6S_8$ and Mo_6S_8 dried sufficiently in air and $Cu_2Mo_6S_8$ and Mo_6S_8 immersed into the THF solvent. Figure 6 shows typical XRD profiles obtained for $Cu_2Mo_6S_8$ and Mo_6S_8 before immersion and during immersion. As is found from Fig. 6(a) and (b), the XRD peaks of $Cu_2Mo_6S_8$ immersed into the THF solvent are found to shift toward lower angle, which indicates that the lattice parameter becomes slightly larger by the immersion. Thus, since it is considered that the solvent infiltration takes some duration, the results shown in Fig. 2(b) can be reasonably understood. Furthermore, when comparing Figs. 6(c) and 6(d), the XRD profile of the immersed Mo_6S_8 is found to change markedly from that of the dried Mo_6S_8. This is one of the most drastically changed sample during immersion, and occasionally such a change is moderate with showing only change in the intensity ratio of

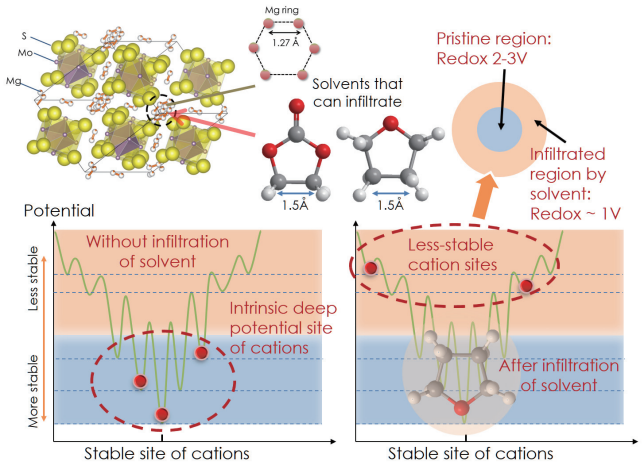

FIG. 5: Schematic illustration of the crystal structure of Chevrel phase and qualitative potential for the cations in the crystal. Without infiltration of the solvent molecules, cations can occupy the most stable site in the crystal, but with infiltration of solvent as a disturbance of the cation site, the cations have no choice but to be located at less stable sites in the crystal.

Mo_6S_8 and $M_xMo_6S_8$ (M denotes a metal cation); the systematic structural change is now under investigation. These changes in the XRD profiles suggest that the THF molecules can infiltrate into the Chevrel crystal and located in the most stable potential site. Currently, the coordination number is unknown, but as judged from the XRD peak shifts, it would be rather small. It was reported that the similar M_6X_8-cluster crystals can contain organic molecules such as THF or acetonitrile,[30, 31] which supports the present swelling phenomenon of the Chevrel phase in terms of the chemical affinity. Thus, we have successfully detected an evidence indicating the solvent infiltration into the Chevrel crystal.

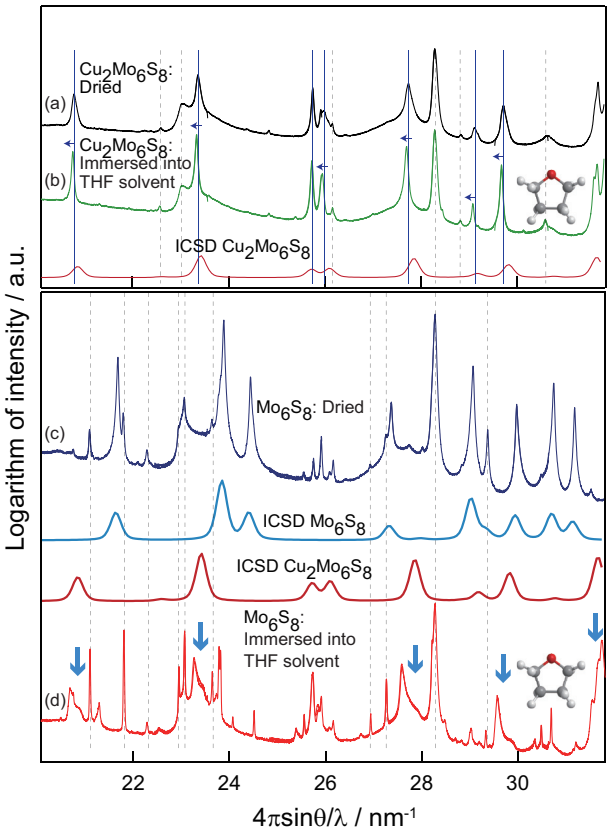

FIG. 6: Typical X-ray diffraction profiles with ICSD data of Mo_6S_8 and $Cu_2Mo_6S_8$; (a) dried $Cu_2Mo_6S_8$, (b) $Cu_2Mo_6S_8$ immersed into THF, (c) dried Mo_6S_8, and (d) Mo_6S_8 immersed into THF. The X-ray diffraction measurements were firstly done for dried samples, and done for the same samples successively immersed in the THF solvent by use of the same capillary. The dashed lines indicate the XRD peaks of the other impurity phases for accurate determination of the peak shift before/after the immersion (the XRD peak of the impurity remains unchanged before/after the immersion).

5. CONCLUDING REMARKS

In this work, we have exposed a new feature of Chevrel compounds that are expected as a positive-electrode material for magnesium rechargeable batteries (MRBs), and shown that the Chevrel compounds demonstrated by Aurbach et al.[5] are still an excellent candidate for the positive electrode. Chevrel compounds possess several cation sites, and the most stable sites would yield the electrode potential of about 3 V vs. Mg/Mg^{2+}. Roughly summarized, the Mo_6S_8 cluster would possess a high redox potential of about 2-3 V vs. Mg/Mg^{2+}. The salient results can be drawn as follows:

1. Above all, the crucial reason why we must reexamine the electrochemical reaction of Chevrel compounds is the thermodynamic conflict that Cu cations can be extracted in a THF solvent at a potential (1.2-1.6 V vs. Mg/Mg^{2+}) lower than the redox potential of metal Cu (about 1.7 V vs. Mg/Mg^{2+}).

2. Therefore, a certain interaction with the electrolyte solvent is indispensable to avoid this thermodynamic contradiction.

3. In this work, we assumed that solvent infiltration into the Chevrel crystal would hinder the proper intercalation/deintercalation of the cations. Namely, infiltration of the solvent molecules into the Chevrel structure (or solvent co-intercalation) would cause the marked decrease of the potential down to about 1.2 V vs. Mg/Mg^{2+}, due to the occupation of the most stable site for the metal cations. We have also detected an evidence from the XRD analysis indicating the swelling phenomenon.

4. In using large molecule solvent or ionic liquids, we have successfully observed the relaxation phenomena as shown in Fig. 3 and 4, where the intercalated cations move to find more stable sites, which directly indicates that the Chevrel compounds have several sites for cations.

Thus, the feasibility of MRB comparable to LIBs would be significantly enhanced with the high potential of the Chevrel compounds, if we would exploit the high-potential cation sites of Chevrel compounds (of about 2-3 V vs. Mg/Mg^{2+}). However, in order to achieve the magnesium battery successfully, we have to find more suitable electrolyte to prevent passivation of Mg electrode surface.

Appendix

The redox potential of Chevrel compound in THF

We have confirmed that the oxidation potential of $Cu_2Mo_6S_8$ in THF is about 1.2-1.6 V vs. Mg/Mg^{2+}, and by many cycles of cyclic voltammetry, Cu in $Cu_2Mo_6S_8$ can be replaced by Mg. This means that the extraction of Cu ions from $Cu_2Mo_6S_8$ can be done at about 1.2-1.6 V vs. Mg/Mg^{2+} in a THF solvent. On the other side, the anodic dissolution of Cu metal occurs above 1.7 V vs. Mg/Mg^{2+} in THF.[13, 14] This magnitude relation is contradictive to thermodynamics, which would be caused by the infiltration of THF molecules into the crystal. Hereafter, let us discuss by regarding that the extraction potential of Cu from $Cu_2Mo_6S_8$ is 1.2 V vs. Mg/Mg^{2+}.

Figure 7 illustrates the electrochemical potential diagram, showing all of the possible reactions including the infiltration of the THF solvent. We consider the electrochemical-equilibrium state, supposing that the oxidative reaction occurs at the working electrode (WE) and the reductive reaction occurs at the reference electrode (RE), namely,

$$\mathrm{WE}: \mathrm{MgMo_3S_4} \leftrightarrow \mathrm{Mo_3S_4} + \mathrm{Mg^{2+}(THF)} + 2\mathrm{e_{WE}}, \quad (2)$$

$$\mathrm{RE}: \mathrm{Mg^{2+}(THF)} + 2\mathrm{e_{RE}} \leftrightarrow \mathrm{Mg}, \quad (3)$$

$$\mathrm{Total}: \mathrm{MgMo_3S_4} + 2\mathrm{e_{RE}} \leftrightarrow \mathrm{Mo_3S_4} + \mathrm{Mg} + 2\mathrm{e_{WE}}, \quad (4)$$

where the cation $Mg^{2+}(THF)$ denotes the THF-solvated magnesium ions, and Mo_3S_4 is used instead of Mo_6S_8, for the sake of simplicity. Then, the electrochemical potential balance in the electrochemical equilibrium is given

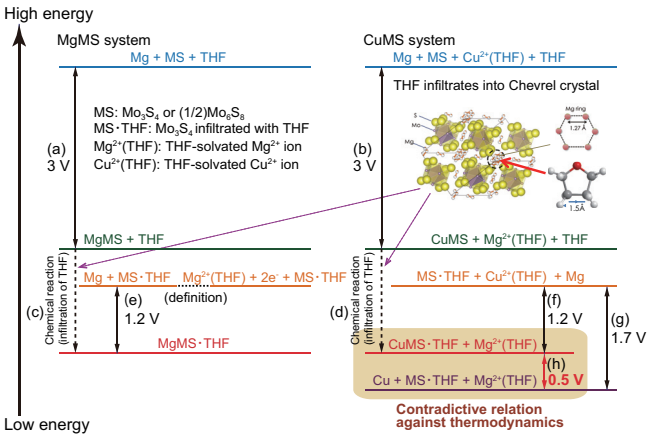

FIG. 7: The electrochemical potential diagram illustrating all of the possible reactions, including the infiltration of the solvent. The electrode-potential standard is defined so as to be $\mu_{\mathrm{Mg^{2+}(THF)}} + 2\mu_{\mathrm{e_{RE}}} = \mu_{\mathrm{Mg}}$ as a reference. The abbreviation MS denotes Mo_3S_4 or $(1/2)Mo_6S_8$.

by

$$\mu_{\mathrm{MgMo_3S_4}} + 2\mu_{\mathrm{e_{RE}}} = \mu_{\mathrm{Mo_3S_4}} + \mu_{\mathrm{Mg}} + 2\mu_{\mathrm{e_{WE}}}, \quad (5)$$

$$-2Femf = 2(\mu_{\mathrm{e_{WE}}} - \mu_{\mathrm{e_{RE}}}) = \mu_{\mathrm{MgMo_3S_4}} - (\mu_{\mathrm{Mo_3S_4}} + \mu_{\mathrm{Mg}}) \equiv 2\mu_{\mathrm{e}}(emf), \quad (6)$$

where Eq. (6) is equivalent to the Nernst equation, F is the Faraday constant, and the electrochemical potential is equivalent to the conventional chemical potential for the neutral materials. Without the infiltration of the solvent, the redox potential of Mo_6S_8 cluster would be about 3 V vs. Mg/Mg^{2+}, that is, we have

$$\mu_{\mathrm{MgMo_3S_4}} - (\mu_{\mathrm{Mo_3S_4}} + \mu_{\mathrm{Mg}}) = 2\mu_{\mathrm{e}}(3\mathrm{V}), \quad (7)$$

where this reaction is denoted by the reaction (a).

Next we consider the case where Cu ions are extracted electrochemically from $Cu_2Mo_6S_8$ in THF with the Mg reference electrode, i.e., the reaction denoted by the reaction (b) in Fig. 7. Then, we consider the electrochemical-equilibrium state as well,

$$\mathrm{WE:\ CuMo_3S_4} \leftrightarrow \mathrm{Mo_3S_4} + \mathrm{Cu^{2+}(THF)} + 2\mathrm{e_{WE}}, \quad (8)$$

$$\mathrm{RE:\ Mg^{2+}(THF)} + 2\mathrm{e_{RE}} \leftrightarrow \mathrm{Mg}, \quad (9)$$

$$\mathrm{Total:\ CuMo_3S_4 + Mg^{2+}(THF)} + 2\mathrm{e_{RE}} \leftrightarrow \mathrm{Mo_3S_4 + Mg + Cu^{2+}(THF)} + 2\mathrm{e_{WE}}. \quad (10)$$

Then, the electrochemical potential balance in the electrochemical equilibrium is given by

$$\begin{aligned} &-2Femf \\ &= \mu_{\mathrm{CuMo_3S_4}} - (\mu_{\mathrm{Mo_3S_4}} + \mu_{\mathrm{Mg}}) + \mu_{\mathrm{Mg^{2+}(THF)}} - \mu_{\mathrm{Cu^{2+}(THF)}} \\ &= \underline{(\mu_{\mathrm{CuMo_3S_4}} - \mu_{\mathrm{Cu^{2+}(THF)}}) - (\mu_{\mathrm{MgMo_3S_4}} - \mu_{\mathrm{Mg^{2+}(THF)}})} \\ &\quad + \{\mu_{\mathrm{MgMo_3S_4}} - (\mu_{\mathrm{Mo_3S_4}} + \mu_{\mathrm{Mg}})\} \\ &\approx 2\mu_{\mathrm{e}}(3\mathrm{V}) = \mu_{\mathrm{MgMo_3S_4}} - (\mu_{\mathrm{Mo_3S_4}} + \mu_{\mathrm{Mg}}), \end{aligned} \quad (11)$$

where the underlined equation would almost equal zero experimentally, because we have the similar redox-potential values in our experimental results, as shown in Fig. 1 in the body text.

On the other hand, in the presence of THF solvent, the solvent molecules infiltrate into the crystal like hydrate, which is denoted by (c) and (d) in Fig. 7; namely,

$$\mathrm{MgMo_3S_4 + THF} \rightarrow \mathrm{MgMo_3S_4 \cdot THF}, \quad (12)$$

$$\mathrm{CuMo_3S_4 + THF} \rightarrow \mathrm{CuMo_3S_4 \cdot THF}, \quad (13)$$

where $\cdot$THF denotes the coordinated solvent in the crystal (but the number of the coordinated molecules is currently unknown). In such cases, we can extract Mg or Cu ions from the crystal at a potential as low as about 1.2 V vs. Mg/Mg^{2+}. The total redox reactions for the respective cases, denoted by (e) and (f) in Fig. 7, are given by

$$\mathrm{MgMo_3S_4 \cdot THF} + 2\mathrm{e_{RE}} \leftrightarrow \mathrm{Mo_3S_4 \cdot THF + Mg} + 2\mathrm{e_{WE}}, \quad (14)$$

$$\mathrm{CuMo_3S_4 \cdot THF + Mg^{2+}(THF)} + 2\mathrm{e_{RE}} \leftrightarrow \mathrm{Mo_3S_4 \cdot THF + Cu^{2+}(THF) + Mg} + 2\mathrm{e_{WE}}. \quad (15)$$

Then, in the electrochemical equilibrium, the Nernst equations are given by

$$\mu_{\mathrm{MgMo_3S_4 \cdot THF}} - (\mu_{\mathrm{Mo_3S_4 \cdot THF}} + \mu_{\mathrm{Mg}}) = 2\mu_{\mathrm{e}}(1.2\mathrm{V}) < 0, \quad (16)$$

$$\mu_{\mathrm{CuMo_3S_4 \cdot THF}} + \mu_{\mathrm{Mg^{2+}(THF)}} - (\mu_{\mathrm{Mo_3S_4 \cdot THF}} + \mu_{\mathrm{Cu^{2+}(THF)}} + \mu_{\mathrm{Mg}}) \approx 2\mu_{\mathrm{e}}(1.2\mathrm{V}) < 0 \quad (17)$$

From Eq. (16), even if the solvent infiltration occurs, $MgMo_3S_4 \cdot$THF is still stable in terms of thermodynamics, because the Gibbs free energy of the compound formation is below zero. Also from Eq. (17), $CuMo_3S_4 \cdot$THF is seemingly stable, but it is not true by the following reason. We have an equation associated with the anodic dissolution of Cu metal with the Mg reference electrode, which is depicted by reaction (g);

$$(\mu_{\mathrm{Mo_3S_4 \cdot THF}} + \mu_{\mathrm{Mg^{2+}(THF)}} + \mu_{\mathrm{Cu}}) - (\mu_{\mathrm{Mo_3S_4 \cdot THF}} + \mu_{\mathrm{Mg}} + \mu_{\mathrm{Cu^{2+}(THF)}}) \approx 2\mu_{\mathrm{e}}(1.7\mathrm{V}), \quad (18)$$

where note that $\mu_{\mathrm{Mo_3S_4 \cdot THF}}$ plays no role in this equation. By subtracting Eq. (18) from (17), consequently, we obtain a very intriguing thermodynamic relation

$$\mu_{\mathrm{CuMo_3S_4 \cdot THF}} - (\mu_{\mathrm{Mo_3S_4 \cdot THF}} + \mu_{\mathrm{Cu}}) \approx 2\mu_{\mathrm{e}}(-0.5\mathrm{V}) > 0. \quad (19)$$

Equation (19) indicates that $CuMo_3S_4 \cdot$THF is unstable or metastable in terms of thermodynamics. On the basis of the present XRD analysis (Fig. 2 in the body text), the Mo_6S_8 compound absorbs the THF solvent, the unstable or metastable $CuMo_3S_4 \cdot$THF compound would be decomposed to $Mo_3S_4 \cdot$THF and Cu in the THF solvent, as shown in reaction (h) in Fig. 7. In other words, from the stand point of the Cu element, it can be expressed that the chemical potential of pure Cu metal is lower than that of the Cu element in the Chevrel compound containing the THF molecules, i.e.,

$$\mu_{\mathrm{Cu}}^{0} < \mu_{\mathrm{Cu}}^{\mathrm{CP \cdot THF}}, \quad (20)$$

which is equivarent to the equation $\mu_{\mathrm{Cu}}^{0} < \mu_{\mathrm{Cu}}^{\mathrm{CP}}$ (in THF) in the body text. Thus, we can understand consistently the experimental fact that we can extract Cu ions from $Cu_2Mo_6S_8$ at such a low potential as 1.2 V vs. Mg/Mg^{2+}, despite the fact that the redox potential of Chevrel compounds is as high as 3 V vs. Mg/Mg^{2+}.

Experimental methods

Sample preparation

$Cu_2Mo_6S_8$ was synthesized in a vacuumed quartz capsule. A mixture of pure Cu (99.9%), Mo (99.9%), S (99.999%) (Furuuchi Chemical Co.) was encapsulated by quartz glass, after vacuumed, the mixture was annealed at 430 °C for 48h and then it was annealed at 1000 °C for 24h to obtain the single-phase sample. The annealed sample was milled and annealed at 1000 °C two times for homogenization, and subsequently the sample was ball-milled to obtain fine particles with a submicron diameter. After the synthesis, the sample was confirmed to have the Chevrel structure by the X-ray diffraction and SEM-EDX analysis. The crystal structure was confirmed to be Chevrel structure, but the composition of sulfur tended to be lower than the stoichiometry composition. To prepare Mo_6S_8, we adopted two ways; (i) $Cu_2Mo_6S_8$ particles were immersed into concentrated hydrochloric acid,[32] and (ii) Cu ions were extracted from $Cu_2Mo_6S_8$ electrode electrochemically in advance.

Structural analysis

For the experiment for the infiltration of the solvent, we used the sample consisting mainly of the Chevrel phase and other impurity phases (e.g., molybdenum sulfide, carbon, PVDF, etc), because the XRD peaks from the other phases is a reference for the accurate determination of the peak position. The powder XRD measurements were done by being capsuled in capillary with or without a tetrahydrofuran solvent. Especially for the powder immersed into THF, the capillary was sealed to prevent the THF molecules escaping from the crystal.

Electrochemical tests

Each composite positive electrode was prepared by coating a Pt plate with a mixture of the Chevrel compound (active material), carbon black (super C 65, as conductive agents), and PVDF (binder) in a weight percent of 8:1:1. Various kinds of beaker cells of three-electrode type were constructed for the electrochemical tests in our glove box whose dew point was below -72°C. All the electrochemical tests were done with galvanostatic/potentiostatic apparatuses (Biologic, SP-300 and VSP-300) in the glove box.

Acknowledgements

This work was supported in part by the Advanced Low Carbon Technology Research and Development Program (ALCA) and by a Grant-in-Aid from the Special Coordination Funds for Promoting Science and Technology commissioned by JST, MEXT of Japan. The authors would like to thank Mrs. Chiharu Hirao for her great experimental help, and are also grateful to Prof. Kuniaki Murase for his encouragement. The crystal structures in the present figures were drawn owing to VESTA 3 software.[33]

[1] W. M. Latimer, *The Oxidation States of the Elements and their Potentials in Aqueous Solutions* (Prentice-hall, INC., Englewood Cliffs, N.J., 1959), second edn.
[2] M. Pourbaix, *Atlas of Electrochemical Equilibria in Aqueous Solutions* (Cebelcor, Brüssel, 1966), second edn.
[3] J. M. Tarascon, M. Armand, *Nature*, 2001, **414**, 359.
[4] S. Yagi, T. Ichitsubo, Y. Shirai, S. Yanai, T. Doi, K. Murase, E. Matsubara, *Journal of Materials Chemistry A*, 2014, **2** 1144-1149.
[5] D. Aurbach, *et al.*, *Nature*, 2000, **407**, 724.
[6] D. Aurbach, *et al.*, *Advanced Materials*, 2007, **19**, 4260.
[7] D. Aurbach, M. D. Levi, E. Levi, *Solid State Ionics*, 2008, **179**, 742.
[8] N. Amir, Y. Vestfrid, O. Chusid, Y. Gofer, D. Aurbach, *Journal of Power Sources*, 2007, **174**, 1234.
[9] E. Levi, M. D. Levi, O. Chasid, D. Aurbach, *Journal of Electroceramics*, 2007, **22**, 13.
[10] E. Levi, Y. Gofer, D. Aurbach, *Chemistry of Materials*, 2010, **22**, 860.
[11] C. Liebenow, *Journal of Applied Electrochemistry*, 1997, **27**, 221.
[12] M. Matsui, *Journal of Power Sources*, 2011, **196**, 7048.
[13] S. Yagi, a. Tanaka, T. Ichitsubo, E. Matsubara, *ECS Electrochemistry Letters*, 2012, **1**, D11.
[14] S. Yagi, A. Tanaka, Y. Ichikawa, T. Ichitsubo, E. Matsubara, *Journal of the Electrochemical Society*, 2013, **160**, C83.
[15] M. Morita, N. Yoshimoto, S. Yakushiji, M. Ishikawa, *Electrochemical and Solid-State Letters*, 2001, **4**, A177.
[16] P. Novák, *Journal of The Electrochemical Society*, 1993, **140**, 140.
[17] T. D. Gregory, R. J. Hoffman, R. C. Winterton, *Journal of The Electrochemical Society*, 1990, **137**, 775.
[18] T. Ichitsubo, T. Adachi, S. Yagi, T. Doi, *Journal of Materials Chemistry*, 2011, **21**, 11764.
[19] J. O. Besenhard, M. Winter, *Chemphyschem : a European journal of chemical physics and physical chemistry*, 2002, **3**, 155.
[20] R. Schöllhorn, M. Kümpers, A. Lerf, E. Umlauf, W. Schmidt, *Materials Research Bulletin*, 1979, **14**, 1039.
[21] T. Ichitsubo, *et al.*, *Journal of Materials Chemistry A*, 2013, **1**, 2567.
[22] K. R. Kganyago, P. E. Ngoepe, C. R. A. Catlow, *Phys. Rev. B*, 2003, **67**, 104103.
[23] Seemingly, the oxidation potential of $Cu_xMo_6S_8$ is low

by about 1 V (i.e., 3 V in aqueous solution to 2 V in THF), but this may be because the difference in the THF-solvation energies between Cu and Mg ions is considered to be smaller than the difference in hydration energies between Cu and Mg aquo-ions.

[24] T. Abe, Private Communication; Y. Orikasa, et al., Abstracts of the Electrochemical Society of Japan, 3C05, 198 (2013).

[25] A. Kitada, Y. Kang, Y. Uchimoto, K. Murase, *Journal of the Electrochemical Society*, 2013, **161**, D102.

[26] Z. W. B. Gao, T. Nohira, R. Hagiwara, *Electrodeposition of Magnesium in Ionic Liquid at 150–200° C, Molten Salts Chemistry and Technology*, John Wiley & Sons, Ltd., 2014, chapt. 5.4.

[27] M. Oishi, T. Ichitsubo, S. Okamoto, S. Toyoda, E. Matsubara, *Journal of The Electrochemical Society*, 161, A943-947 (2014).

[28] At the electrodeposition potential of Cs, both of Cs and Mg tend to be deposited, then the redox potential of Mg was found to be about 0.8-0.9 V higher than that of Cs, and the redox potential difference between Cs and Li is about 0.4 V, and hence we have the converted potential vs. Mg/Mg^{2+} by subtracting about 0.5 V from the potential vs. Li/Li^{+}.

[29] T. Ichitsubo, et al., *Journal of Materials Chemistry*, 2011, **21**, 2701.

[30] C. A. Goddard, J. R. Long, R. H. Holm, *Inorganic Chemistry*, 1996, **35**, 4347.

[31] S. Kamiguchi, H. Imoto, T. Saito, T. Chihara, *Inorganic Chemistry*, 1998, **37**, 6852.

[32] E. Lancry, E. Levi, A. Mitelman, S. Malovany, D. Aurbach, *Journal of Solid State Chemistry*, 2006, **179**, 1879.

[33] K. Momma, F. Izumi, *Journal of Applied Crystallography*, 2011, **44**, 1272.